

# Nanoscale

Accepted Manuscript



This is an *Accepted Manuscript*, which has been through the Royal Society of Chemistry peer review process and has been accepted for publication.

*Accepted Manuscripts* are published online shortly after acceptance, before technical editing, formatting and proof reading. Using this free service, authors can make their results available to the community, in citable form, before we publish the edited article. We will replace this *Accepted Manuscript* with the edited and formatted *Advance Article* as soon as it is available.

You can find more information about *Accepted Manuscripts* in the [Information for Authors](#).

Please note that technical editing may introduce minor changes to the text and/or graphics, which may alter content. The journal's standard [Terms & Conditions](#) and the [Ethical guidelines](#) still apply. In no event shall the Royal Society of Chemistry be held responsible for any errors or omissions in this *Accepted Manuscript* or any consequences arising from the use of any information it contains.

## ARTICLE

## A value-added exopolysaccharide as a coating agent for MRI nanoprobos

Cite this: DOI: 10.1039/x0xx00000x

Susana I. C. J. Palma<sup>a</sup>, Carlos A. V. Rodrigues<sup>b</sup>, Alexandra Carvalho<sup>c</sup>, Maria del Puerto Morales<sup>d</sup>, Filomena Freitas<sup>a</sup>, Alexandra R. Fernandes<sup>e,f</sup>, Joaquim M.S. Cabral<sup>b</sup>, Ana C. A. Roque<sup>a\*</sup>

Received 00th January 2012,  
Accepted 00th January 2012

DOI: 10.1039/x0xx00000x

[www.rsc.org/](http://www.rsc.org/)

Fucopol, a fucose-containing exopolysaccharide (EPS) produced by the bacterium *Enterobacter* A47 DSM 23139 using glycerol as a carbon source, was employed as a new coating material for iron oxide magnetic nanoparticles (MNP). The coated particles were assessed as nanoprobos for cell labeling by Magnetic Resonance Imaging (MRI). The MNP were synthesized by a thermal decomposition method and transferred to aqueous medium by ligand-exchange reaction with meso-2,3-dimercaptosuccinic acid (DMSA). Covalent binding of EPS to DMSA-stabilized nanoparticles (MNP-DMSA) resulted in a hybrid magnetic-biopolymeric nanosystem (MNP-DMSA-EPS) with a hydrodynamic size of 170 nm, negative surface charge at physiological conditions and transverse to longitudinal relaxivities ratio,  $r_2/r_1$ , of 148. *In vitro* studies with two human cell lines (colorectal carcinoma - HCT116 - and neural stem/progenitor cells - ReNcell VM) showed that EPS promotes internalization of nanoparticles in both cell lines. *In vitro* MRI cell phantoms also showed superior performance of MNP-DMSA-EPS in ReNcell VM, for which iron dose-dependent MRI signal drop was obtained at relatively low iron concentrations (12 - 20  $\mu\text{g Fe/ml}$ ) and short incubation time. Furthermore, ReNcell VM multipotency was not affected by culture in the presence of MNP-DMSA or MNP-DMSA-EPS for 14 days. Our study suggests that Fucopol-coated MNP represent useful cell labeling nanoprobos for MRI.

## ARTICLE

## Introduction

Iron oxide magnetic nanoparticles (MNP) represent an interesting platform with application in several areas, particularly in the biotechnological and biomedical fields, due to their biocompatibility and superparamagnetic properties. In the last two decades, a large number of research studies evaluated the use of MNPs in magnetic resonance imaging (MRI), in hyperthermia, as multimodal imaging agents, as nanovectors for drug and gene delivery, or in a combination of these imaging and therapeutic functions to build theranostic nanosystems.<sup>1-3</sup> Interactions between biological environment and MNPs are mediated by the coating material and functionalization, which allow to tailor the MNPs in terms of specific cell-type targeting, drug release, cellular uptake, multifunctionality or *in vivo* stealth properties. Hydrophilic coatings, usually composed of small molecules (e.g. meso-2,3-dimercaptosuccinic acid (DMSA)) or polymers, either synthetic (e.g. polyethyleneglycol (PEG)) or natural (e.g. dextran), are preferred due the compatibility with biological media and the ability to provide colloidal stabilization to the nanosystem.

Clinical application of MNPs is subjected to approval by health regulatory agencies (eg. Food and Drug Administration - FDA), which require the particles to be biodegradable following their administration.<sup>4</sup> Since inert synthetic coatings or encapsulation matrices are mostly not biodegradable, polysaccharides are appealing alternative materials. They are abundant in nature, hydrophilic, biodegradable and generally accepted as biocompatible. In addition, availability of functional groups for chemical modification<sup>5</sup> make polysaccharide-coated MNPs versatile nanoplatfroms. Indeed, iron oxide based commercial MRI contrast agents are typically coated with dextran or chemically modified versions of this bacterial polysaccharide (e.g. Ferumoxides (Feridex/Endorem) from Advanced Magnetics (USA) and Ferucarbotran (Resovist), from Bayer Shering Pharma AG (Germany)).<sup>6</sup> Exopolysaccharides (EPSs) are polysaccharides secreted to the extracellular environment by many microorganisms. The extracellular nature of EPS simplifies their extraction process. EPS are mostly composed of neutral monosaccharides but in some cases amino-sugars and/or acidic sugars are also part of the composition. Some non-carbohydrate substituents (such as acetate, pyruvate, succinate, and phosphate) are also found in many microbial EPS.<sup>7</sup> Although dextran is still the most used microbial polysaccharide to coat MNPs for imaging, diagnosis and treatment<sup>8</sup>, other EPSs have been studied and reviewed in the literature.<sup>5</sup> For example, multifunctional MNP bearing a targeting moiety and an anticancer drug were developed based on EPS (mauran and gellan) coatings and showed potential for

imaging and magnetic hyperthermia.<sup>9</sup> Similarly, pullulan derived coatings originated MNPs with potential for magnetic hyperthermia in human nasopharyngeal epidermal carcinoma cell line<sup>10</sup> and MRI labeling of rat mesenchymal stem cells.<sup>11</sup> Fucopol is an EPS produced by *Enterobacter* A47 DSM 23139 using glycerol as the sole carbon source.<sup>7</sup> It is composed of fucose, galactose, glucose, pyruvate, succinate and acetate in the molar ratios 1.6:1.3:1.1:1.2:0.7:1.5. The polymer possesses a residual protein fraction of 5 wt.%.<sup>7</sup> This environmentally-friendly, sustainable EPS is considered a high added value product because, in addition to good flocculating and emulsion stabilizing properties, it is rich in fucose, which is one of the rare sugars, difficult to obtain but with many applications, from pharmaceutical to cosmetics.<sup>7</sup> Preparations containing fucose, fucose-containing oligomers or polymers were shown to have biological properties such as anti-carcinogenic, anti-inflammatory and induction of neuronal growth.<sup>7,12</sup> Our research group has previously shown the good performance of Fucopol as a coating material of magnetic particles employed in human antibody purification.<sup>13</sup> Due to the biological importance of fucose and the properties of EPS, Fucopol was explored as a coating material for magnetic nanoparticles intended for biomedical applications, in particular, as MRI contrast agents.

Fucopol was covalently bound to meso-2,3-dimercaptosuccinic acid-functionalized MNP and the resulting nanosystem (MNP-DMSA-EPS) was characterized regarding its composition, size, magnetic and relaxometric properties. After evaluation of MNP-DMSA-EPS *in vitro* cytotoxic potential, the respective cell labeling efficacy was studied in two human cell lines (a colorectal cell line and a neural stem/progenitor cell line). Prussian blue staining, fluorescence microscopy, chemical quantification of iron internalization and *in vitro* MRI of cell phantoms were employed to assess the efficacy of the nanoprobos.

## Experimental Methods

### Materials

Fucopol exopolysaccharide (EPS)<sup>7</sup> was produced by cultivation of the bacterium *Enterobacter* A47 DSM 23139, using glycerol as the sole carbon source, under controlled bioreactor conditions, as previously described.<sup>11</sup> The polymer was recovered from the culture broth by dialysis of the cell-free supernatant and freeze-dried.

### Synthesis and phase transfer of iron oxide magnetic nanoparticles (MNP-DMSA)

Hydrophobic iron oxide magnetic nanoparticles were synthesized by the thermal decomposition of iron tri(acetylacetonate) in benzyl ether using 1,2-tetradecanediol as reducing agent, and oleic acid and oleylamine as surfactants.<sup>14</sup> To render these MNP hydrophilic a ligand-exchange reaction with DMSA was employed.<sup>15</sup> Briefly, a toluene dispersion of hydrophobic MNP was mixed with a solution of DMSA in dimethylsulfoxide (DMSO). After 48 h incubation at room temperature, the solvent containing the oleic acid and oleylamine was discarded and the black hydrophilic nanoparticles were re-dispersed in ethanol. After several washes by centrifugation the nanoparticles were re-dispersed in milliQ water, basified to pH 10 and dialyzed against milliQ to provide the final DMSA coated MNP (MNP-DMSA).

### Preparation of EPS-coated magnetic nanoparticles (MNP-DMSA-EPS)

Fucopol was covalently coupled onto the hydrophilic MNP-DMSA using carbodiimide chemistry. A Fucopol solution (5 mg/ml, in phosphate buffer, 0.1 M, pH 7.6) was prepared and centrifuged to remove any unsolubilized polymer fraction. Only the supernatant ( $3.7 \pm 0.7$  mg Fucopol/ml, quantified through the anthrone test<sup>16</sup>) was used for the coating reaction. To activate the carboxylic acid groups of DMSA, N-(3-Dimethylaminopropyl)-N'-ethylcarbodiimide (EDC) and N-Hydroxysuccinimide (NHS) were added to 2 ml of MNP-DMSA (2 mg/ml, in MES buffer, 0.1 M, pH 6) at the concentration of 2 mM and 50 mM, respectively, followed by 15 min of incubation in a rotating agitator (Stuart, SB3) (20 rpm) at room temperature. Then, the pH was adjusted to 7.6 and the activated MNP-DMSA were added dropwise to the polymer solution under vigorous (700 – 1000 rpm) magnetic agitation. The reaction continued in a rotating agitator (20 rpm) overnight at room temperature. MNP-DMSA-EPS were recovered by several cycles of centrifugation (9000 rcf, 15 min) and replacement of the supernatant by milliQ water. The larger aggregates were magnetically removed using a magnetic separator for microcentrifuge tubes (Bilatest M12+12, Sigma Aldrich).

### Characterization of magnetic nanoparticles

Particle size and shape were characterized by Transmission Electron Microscopy (TEM) using a 100-kV JEOL JEM1010 microscope equipped with a Gatan Orius 200 SC digital camera. Hydrodynamic size ( $d_h$ ) and zeta potential of the particles were determined using a Nanosizer ZS (Malvern). The mean value of the intensity-weighted size distribution, measured at pH 7, was used as  $d_h$ . Zeta potential variation with pH was measured in a 0.01 M  $KNO_3$  solution ( $HNO_3$  or KOH solutions were used for pH adjustment). To evaluate the particles' hydrodynamic diameter stability in physiological

conditions, we have analyzed the Z-Average value of samples dispersed in both Phosphate Buffered Saline (0.01 M; with 0.15 M NaCl, pH 7.4) (PBS) and Dulbecco's Modified Eagle's culture medium supplemented with bovine serum. Two time points were studied:  $t = 0$  h (at the moment of the nanoparticles dispersion) and  $t = 2$  h (2 h after the preparation of the nanoparticles dispersion). Inductively coupled plasma - atomic emission spectroscopy (ICP-AES) (Horiba Jobin-Yvon, Ultima) was used to determine the iron content of the MNP samples. Fourier transform infrared (FTIR) spectra were acquired using a Nicolet 20 SXC FTIR. Thermogravimetric analysis (TGA) of MNP-DMSA and MNP-DMSA-EPS powder was carried out in a Seiko TG/DTA 320 U, SSC 5200 thermobalance.

Magnetization measurements were performed using a vibrating sample magnetometer (VSM) (MagLab VSM, Oxford Instruments). Magnetization loops were measured at 250 K, corrected by subtracting the diamagnetic contribution of the dispersants (50  $\mu$ l) and the sample holder, and normalized to the saturation magnetization value ( $m_{max}$ ) of each sample.

The relaxometric properties of MNP-DMSA-EPS were evaluated in a 7 T NMR Bruker Avance III Spectrometer at 25°C. Water suspensions of MNP-DMSA-EPS at different iron concentrations were prepared. Longitudinal relaxation time  $T_1$  was measured using an inversion recovery pulse sequence with TR between 3 and 10 s. Transverse relaxation time  $T_2$  was measured using a Call-Purcell-Meiboom-Gill pulse sequence with TE of 1 ms and the number of echoes needed to cover a time interval of about 10 times  $T_2$ . Longitudinal ( $R_1 = 1/T_1$ ) and transversal ( $R_2 = 1/T_2$ ) relaxation rates were plotted against iron concentration and a linear behavior was found. The lines slopes are the longitudinal ( $r_1$ ) and transverse ( $r_2$ ) relaxivities, that measure the efficiency of the nanoparticles as MRI contrast agents.  $T_2$ -weighted MRI phantom images of MNP-DMSA-EPS water suspensions at 0.1, 0.4, 0.8 and 1 mM (Fe) were obtained with a multi-echo image sequence ( $T_R = 5$  s;  $T_1 = 8$  ms).

### Cell culture and labeling

Two adherent human cell lines were used in this work: a colorectal carcinoma cell line (HCT116) and a neural stem/progenitor cell line (ReNcell VM). HCT116 cells were cultured in Dulbecco's modified Eagle's medium (DMEM, Life Technologies) supplemented with 10% (v/v) fetal bovine serum (Life Technologies) and 1% (v/v) of penicillin-streptomycin (Life Technologies) at 37 °C with 99% relative humidity and 5%  $CO_2$ . ReNcell VM cells were seeded in tissue culture plates or glass coverslips sequentially coated with poly-L-ornithine (Sigma-Aldrich, 15  $\mu$ g/ml, 30 min at 37°C) and laminin (Sigma-Aldrich, 10  $\mu$ g/ml, 3 h at 37°C), and cultured in DMEM/F12 medium supplemented with 20 ng/ml EGF (Preprotech), 20 ng/ml FGF-2 (Peprotech), 1% N2 supplement (Life Technologies), 20  $\mu$ l/ml B27 supplement (Life Technologies), 20  $\mu$ g/ml additional insulin (Sigma-Aldrich), 1.6 g/l additional glucose (Sigma-Aldrich) and 1%

penicillin/streptomycin at 37°C and 5% CO<sub>2</sub> humidified environment.

Cells were incubated under the standard conditions referred above until 70-80% confluence was reached. Cells were then labeled by incubating with the corresponding culture medium with different concentrations of MNPs for 48h (in the case of HCT116)<sup>17</sup> or for 4h followed by 24h recovery in fresh culture medium (in the case of ReNcell VM).<sup>18,19</sup> Nanoparticles were sterilized by filtration with a sterile membrane filter of 0.20 µm pore diameter (MNP-DMSA) or by autoclaving 20 min at 120°C (MNP-DMSA-EPS).

### Multi-lineage differentiation of ReNcell VM

ReNcell VM differentiation into neuronal and glial lineages was induced by changing the culture medium and withdrawing EGF and FGF-2. Cells were cultured using a 1:1 mixture of DMEM/F12 supplemented with N2 (1x) and Neurobasal medium (Life Technologies) supplemented with B27 (1x). Medium was changed every 2-3 days. The differentiation process was carried out for 14 days.

Differentiation was evaluated by immunostaining for the neuronal marker β-III Tubulin (Tuj1, Covance) and for astrocyte marker glial fibrillary acidic protein (GFAP, Millipore). Cells were fixed with paraformaldehyde (PFA, 4%, Sigma) for 30 min at room temperature, and then washed twice with phosphate buffered saline (PBS, Life Technologies). Cells were incubated for 45 min at room temperature with blocking solution (PBS with 0,1% Triton X-100 and 10% normal goat serum (NGS)). Afterwards, cells were incubated at 4°C overnight with the primary antibodies diluted (Tuj1 1:2000, GFAP 1:100) in staining solution (PBS with 0,1% Triton X-100 and 5% NGS). Cells were then washed once with PBS and incubated with the appropriate secondary antibody (Life Technologies, dilution 1:500) for 1 h at room temperature in a dark container. Finally, cells were washed once with PBS, incubated with DAPI (1.5 µg/ml in PBS, Sigma) for 2 min at room temperature and washed twice with PBS. The stained cells were visualized under a fluorescence microscope (Leica DMI 3000B).

### Cytotoxicity evaluation

The impact of nanoparticles and Fucopol on the viability of HCT116 and ReNcell VM cultures was evaluated using a standard 3-(4,5-dimethylthiazol-2-yl)-2,5-diphenyl tetrazolium bromide (MTT) colorimetric assay as described previously.<sup>20</sup> Briefly, cells were seeded in 96 well plates at 7.5 ×10<sup>3</sup> cells/well and labeled with MNP-DMSA and MNP-DMSA-EPS at different iron concentrations. Cells were also incubated with EPS at concentrations corresponding to the EPS content in MNP-DMSA-EPS at the chosen iron concentrations (calculated from TGA data).

After labeling, the culture medium was removed and replaced by fresh medium containing MTT (0.45 mg/ml). After 3 h of incubation in standard culture conditions, the medium was replaced by dimethyl sulfoxide (DMSO, Sigma-Aldrich) to

dissolve the formazan crystals obtained as a result of MTT metabolism. The absorbance of the wells at 540 nm (abs@450nm) and 630 nm (abs@630nm) was measured in a microplate reader (Microplate Titre Infinite F200, TECAN Spectra). Cell viability was calculated using the equation:

$$\text{cell viability (\%)} = \frac{(\text{abs@540nm} - \text{abs@630nm})_{\text{sample}}}{(\text{abs@540nm} - \text{abs@630nm})_{\text{control}}} \times 100 \quad (1)$$

Where *sample* refers to cells incubated with nanoparticles or EPS, and *control* refers to cells without nanoparticles or EPS. Determination of the half maximal inhibitory concentration (IC<sub>50</sub>) for each nanoparticle type and EPS was performed by fitting the viability data to a dose-response sigmoidal curve.<sup>20</sup>

### Identification of cellular iron by Prussian blue staining

For bright field microscopy observation, cells were seeded in coverslips on the bottom of the wells of 24-well plates at 1×10<sup>5</sup> cells/well, incubated in standard conditions and labeled with MNP-DMSA (55 µg Fe/ml for HCT116 and 50 µg Fe/ml for ReNcell VM) or MNP-DMSA-EPS (82 µg Fe/ml for HCT116, and 16 µg Fe/ml for ReNcell VM). After labeling, cells were stained with Prussian blue for iron identification and counterstained with neutral red as described previously<sup>20</sup> and visualized by bright field microscopy. Slides were observed using an Olympus CX41 microscope equipped with an Olympus SC30 camera.

### Intracellular localization of magnetic nanoparticles

To determine the intracellular location of MNP-DMSA-EPS, fluorescent labeling of lysosomes with GFP was performed and preparations were observed under fluorescence and bright field microscopy to look for co-localization of nanoparticles and lysosomes. HCT116 and ReNcell VM cells were seeded in coverslips at the bottom of 35 mm petri dishes or wells of 24-well plate, at 1×10<sup>4</sup> cells/cm<sup>2</sup>, cultured in standard conditions and labeled with MNP-DMSA-EPS at 82 µg Fe/ml and 16 µg Fe/ml, respectively. 20 h before the end of the incubation time, Cell-Light Lysosomes-GFP, BacMam 2.0 reagent (Life Technologies) was added directly to the cells (25 particles per cell) and left incubating overnight. Cells were, then, washed with PBS and fixed with ice-cold paraformaldehyde (4% v/v in PBS). The preparation was air dried and mounted in the microscope slide using 5 µl of DAPI solution. Slides were observed using an Olympus BX51 microscope equipped with an Olympus DP50 camera and the Cell F View Image System Software.

### Iron quantification

Cells were plated at 1×10<sup>5</sup> cells/well in 24-well plate wells, cultured in standard conditions and labeled with MNP-DMSA (54 µg Fe /ml for HCT116, and 46 µg Fe /ml for ReNcell VM) or MNP-DMSA-EPS (57 µg Fe/ml for HCT116, and 16 µg Fe/ml for ReNcell VM), as quantified by ICP in the culture

media. After labeling, the supernatant was collected from each well and cells were detached from the wells, re-suspended in culture medium, counted using a haemocytometer and centrifuged for 10 min at 5000 rpm. Cell pellet (fraction 1), cell supernatant (fraction 2) and well supernatant (fraction 3) were separately digested with 100  $\mu$ l of *aqua regia* for 30 min at 90°C, diluted to 1 ml with milliQ water and analyzed separately for iron by ICP-AES. The iron in the cellular fraction (sum of fraction 1 and fraction 2) was normalized to the number of cells and to the total mass of iron (sum of the three fractions).

### *In vitro* MRI of cell phantoms

Cells were plated in 24-well plates at  $1 \times 10^5$  cell/well, cultured in standard conditions and labeled with MNP-DMSA-EPS at three increasing iron concentrations (61.5, 82 and 102.5  $\mu$ g Fe/ml for HCT116 cells and 12, 16 and 20  $\mu$ g Fe/ml for

ReNcell VM cells). After labeling, cells were prepared for MR imaging as described previously.<sup>20</sup> Briefly, cells were washed, collected by centrifugation, fixed with cold paraformaldehyde, re-dispersed in PBS and counted using a haemocytometer.  $3 \times 10^5$  HCT116 cells and  $5.7 \times 10^5$  ReNcell VM cells were dispersed in 0.1 ml of PBS, mixed with 0.2 ml aliquots of fresh 0.75% (m/v) agarose and transferred to 5 mm diameter NMR tubes for imaging after solidifying. T2-weighted MR images were obtained in a magnetic field of 7 T, at 25 °C, using a Bruker Avance III Spectrometer (160 G/cm imaging gradient) and a Flash imaging sequence (TR = 110 ms, TE = 1.7 ms, with a 20° excitation angle and NEX of 32). MRI signal was quantified using ImageJ software (National Institutes of Health) to calculate the histogram, the average pixel value and the integrated density (sum of all pixel values divided by the average pixel value) over a 6 mm<sup>2</sup> circular region of interest placed in the center of each cell phantom image.

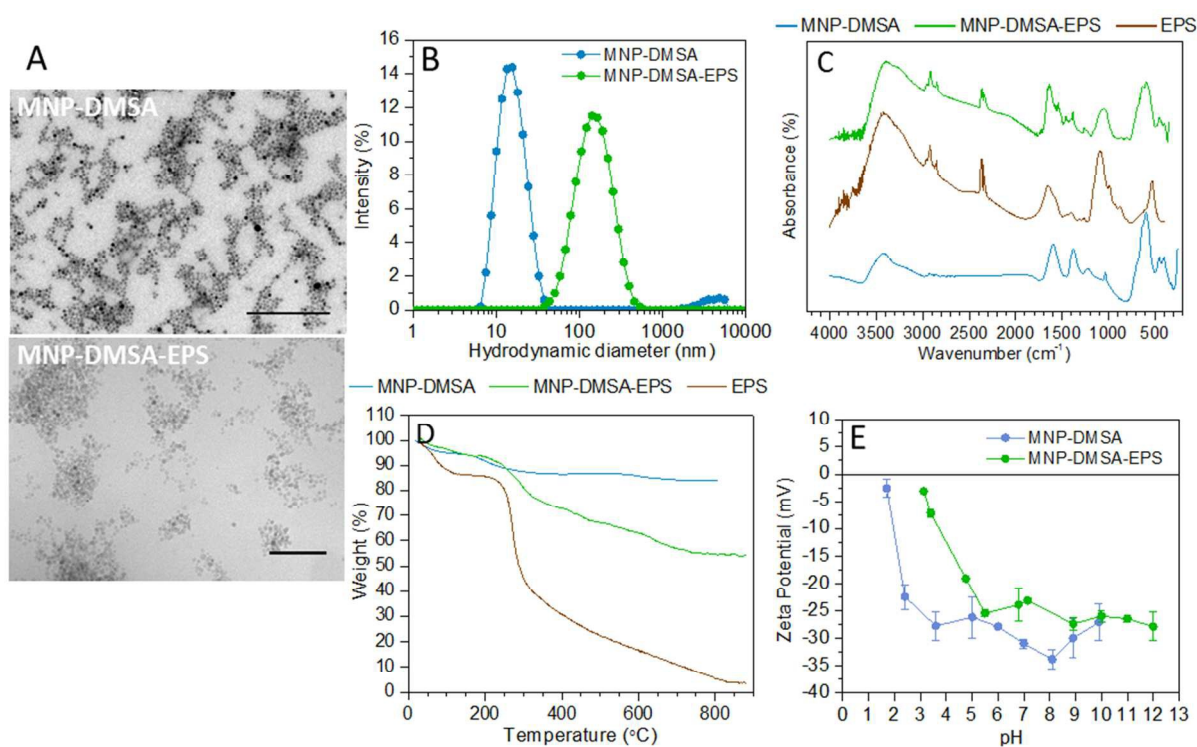


Figure 1 Characterization of size and composition of the produced nanoparticles. (A) Morphology of MNP-DMSA and MNP-DMSA-EPS by TEM (scale bars: 100 nm); (B) hydrodynamic diameters; (C) FTIR spectra of particles and EPS; (D) thermogravimetric analysis of particles and EPS; (E) evolution of zeta potential with pH.

## Results and Discussion

### Particle size, composition and surface chemistry

Iron oxide magnetic nanoparticles were synthesized by thermal decomposition of iron(III) acetylacetonate in benzyl ether in the presence of tetradecanediol, oleic acid and oleylamine. The resulting particles are monodisperse but hydrophobic. To render them hydrophilic, the oleic moieties originally at the surface of the particles were replaced by DMSA through a ligand-exchange reaction,<sup>15</sup> leaving carboxylic acid groups at the surface of the particles. The carboxylate functionalities were

then used as chemical anchors to couple Fucopol exopolysaccharide (EPS) through the amine groups of the associated protein. EDC/NHS chemistry was chosen to promote the covalent conjugation of the carboxylic and amine groups. During the coating reaction, and due to its high molecular weight ( $5.8 \times 10^6$  g/mol)<sup>7</sup>, Fucopol forms a network that entraps multiple cores of MNP-DMSA (which alone present  $d_h = 15 \pm 2$  nm;  $d_{core} = 7 \pm 1$  nm), forming aggregates with hydrodynamic diameter of  $168 \pm 40$  nm (Figure 1 A and B) and polydispersity index of 0.25. Each aggregate (particle) is thus estimated to contain 14000 iron oxide magnetic cores. Despite being pointed

out as a drawback of polysaccharides, the natural batch-to-batch variability of Fucopol was not a problem in this work. Namely, no influence on MNP-DMSA-EPS size, morphology and colloidal stability was observed when different batches of polymer were employed.

Dispersion of the nanoparticles in physiological media like PBS or cell culture medium supplemented with fetal bovine serum (FBS) resulted in aggregation and increase of polydispersity (Figure S3A and S3B, respectively). Interestingly, while MNP-DMSA maintain the Z-Average in PBS and culture medium, MNP-DMSA-EPS show stronger aggregation in PBS than in culture medium and, after 2 h of incubation in the later conditions, tend to their native Z-Average ( $139 \pm 35$  nm, measured in water at pH 7). This behavior thus shows that interaction with the dispersant is a dynamic process. FTIR spectrum of MNP-DMSA-EPS (Figure 1C) presents, in the regions of  $600\text{ cm}^{-1}$  and  $400\text{ cm}^{-1}$ , the typical bands from Fe-O bonds vibrations in the spinel structure of magnetite.<sup>21</sup> Compared to MNP-DMSA, extra bands of weak intensity attributed to the oxidation of magnetite to maghemite appear together with these two main bands, in particular in the  $600\text{ cm}^{-1}$  region, for MNP-DMSA-EPS.<sup>21</sup> The coating reaction thus has an effect on the iron oxide crystalline structure at the surface of the particles. FTIR was also used to confirm the presence of the EPS shell on the nanoparticles. Indeed, the Fucopol fingerprint band (the envelope between approximately  $1200$  and  $900\text{ cm}^{-1}$ )<sup>7</sup> is also present in MNP-DMSA-EPS spectrum and not in that of MNP-DMSA. This band corresponds to skeletal C-O and C-C vibrations bands of glycosidic bonds and pyranoid rings.<sup>22</sup> Also, the less intense band at  $1265\text{ cm}^{-1}$ , present in both EPS and MNP-DMSA-EPS spectra, can be associated with the vibration of C-O-C of acyl groups.<sup>22</sup> The band present at  $\sim 1650\text{ cm}^{-1}$  in MNP-DMSA-EPS may be attributed to contributions from C=O stretching vibrations from the peptide bond (amide I band)<sup>23</sup> formed through the covalent conjugation of EPS amine and DMSA carboxyl groups. It may also be associated with the vibrations of C=O from carboxylates present in EPS. The appearance of a band at around  $1540\text{ cm}^{-1}$  in the spectrum of MNP-DMSA-EPS that resembles the amide II band (associated with N-H bending and C-N stretching vibrations in amide bonds)<sup>23</sup>, confirms the effectiveness of the covalent conjugation of EPS onto the nanoparticles.

The TGA curves (Figure 1D) also support the presence of EPS on MNP-DMSA-EPS due to the similar weight loss profiles of this sample and free EPS between  $200^\circ\text{C}$  and  $800^\circ\text{C}$  (a first accentuated step at  $275^\circ\text{C}$  followed by a less pronounced and longer step). The curves of MNP-DMSA and MNP-DMSA-EPS present an initial weight loss of 5% due to water removal, followed by loss of DMSA or DMSA and EPS. MNP-DMSA curve reveals that DMSA is lost at around  $200^\circ\text{C}$  and corresponds to approximately 11% of MNP-DMSA total weight. After coating with EPS, 40% of the nanoparticles weight is lost (Figure 1D), which means that EPS constitutes 29% of the nanoparticles total weight. Taking in consideration the EPS molecular weight, the density of  $\text{Fe}_2\text{O}_3$  ( $5.24\text{ g/cm}^3$ ) and the number of cores per aggregate calculated above, one

can estimate 725 EPS molecules per aggregate, that corresponds to 0.05 EPS molecules per core.

Due to the presence of succinate, pyruvate and glucuronic acid in the composition of EPS<sup>7</sup>, EPS-coated nanoparticles maintain negative zeta potential for pH values higher than 3 (Figure 1E). However, the presence of salt in solution affects the zeta potential. We observe a value of  $-32 \pm 4$  mV in milliQ water, at pH 7, which increases to  $-23.2 \pm 0.2$  mV when the dispersion contains 0.01 M of  $\text{KNO}_3$ . This shows that colloidal stability does not depend only on steric interactions between the polymer chains but also on electrostatic interactions. It is known that interaction of nanoparticles with complex biological fluids leads to the formation of a protein corona that changes the particles' surface properties and may influence their stability and interaction with cells.<sup>24-26</sup> In this work, besides causing an initial aggregation of MNP-DMSA and MNP-DMSA-EPS, the interaction of particles with cell culture medium supplemented with FBS increased their surface charge to values near neutral (Figure S3D) probably due to adsorption of proteins and other biomolecules that compose the culture medium onto the surface of the MNPs.

#### Magnetic properties and relaxivities measurements

The magnetization measurements at room temperature (Figure 2A) revealed that MNP-DMSA and MNP-DMSA-EPS present superparamagnetic behavior. Wasp-waist loops are observed for both samples (Figure 2A and Figure S1), but in larger extent for MNP-DMSA-EPS. This indicates that the iron cores are composed of two distinct magnetic phases<sup>27,28</sup> and that the EPS coating reaction magnified the differences in magnetic anisotropy of those two phases. This is consistent with a core-shell structure for the magnetic cores in MNP-DMSA-EPS, composed of a well crystalline magnetite core and a more oxidized surface layer, as suggested by the FTIR spectra (Figure 1C), and further distorted by the polymer coupling as suggested by the saturation at larger fields (Figure 2A). When the exchange between a soft magnetic material and a hard material is positive, the loop is conventional. However, for negative (antiferromagnetic) exchange, the wasp-waist loop is obtained.<sup>28</sup>

To evaluate the potential of the EPS-coated nanoparticles as MRI contrast agent we have evaluated their ability to change the proton longitudinal ( $T_1$ ) and transverse ( $T_2$ ) relaxation times at room temperature. Figure 2B shows the linear dependence found between the longitudinal ( $R_1=1/T_1$ ) and transverse ( $R_2=1/T_2$ ) proton relaxation rates and iron concentration for MNP-DMSA and MNP-DMSA-EPS in water suspensions.

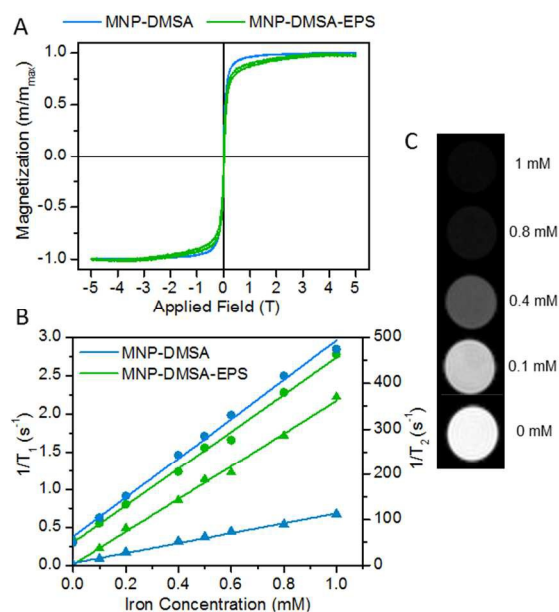


Figure 2. Evaluation of magnetic and relaxometric properties. (A) Magnetization loops of the nanoparticles before and after coating with EPS, measured at 250 K; (B) Determination of longitudinal ( $r_1$ ) and transversal ( $r_2$ ) relaxivity values before and after coating with EPS (circles:  $1/R_1$ ; triangles:  $1/R_2$ ); (C) *In vitro*  $T_2$ -weighted MRI phantoms of water dispersions of MNP-DMSA-EPS at different iron concentrations.

From the slope of these linear relations, we conclude that MNP-DMSA-EPS presents low longitudinal relaxivity,  $r_1$ , ( $2.4 \text{ mM}^{-1} \text{ s}^{-1}$ ) and high transverse relaxivity,  $r_2$ , ( $361 \text{ mM}^{-1} \text{ s}^{-1}$ ) as it is typical of superparamagnetic nanoparticles, which can act as negative MRI contrast agents (decrease in MRI signal, i.e., a darkening effect). Compared to MNP-DMSA ( $r_1 = 2.6 \text{ mM}^{-1} \text{ s}^{-1}$ ,  $r_2 = 110 \text{ mM}^{-1} \text{ s}^{-1}$ ), MNP-DMSA-EPS maintain the longitudinal value but increase the transverse relaxivity (Figure 2B). The larger transverse relaxivity could be associated with the clustered nature of MNP-DMSA-EPS because in the aggregation of several small nanoparticles increases the effective magnetic size of the system<sup>29,30</sup>. However, the peak for the blocking temperature in the zero field cooling curve (ZFC) of MNP-DMSA-EPS (Figure S2) is not significantly shifted to the right in comparison to the uncoated nanoparticles, suggesting that the aggregation alone does not justify the increase in  $r_2$ . On the other hand, significant dipolar interactions do take place within MNP-DMSA-EPS as ZFC curve keeps increasing after the blocking temperature, which also has the effect of increasing the effective magnetization of the nanoparticles and, consequently, can lead to the increase of the transverse relaxivity value. Comparison of MNP-DMSA-EPS with similar hydrodynamic size commercial MRI agent Endorem/Feridex ( $d_h = 120 - 180 \text{ nm}$ ) reveals that our nanoparticles present a much higher  $r_2$  value and similar  $r_1$  ( $r_1 = 2.2 \text{ mM}^{-1} \text{ s}^{-1}$  and  $r_2 = 182 \text{ mM}^{-1} \text{ s}^{-1}$  for Endorem/Feridex) at the same magnetic field<sup>31</sup>, what makes the ratio  $r_2/r_1$  1.8 times larger for our particles (148 vs. 83). This ratio is used to quantify and compare the efficacy of a negative contrast agent for MRI. For negative contrast agents, larger  $r_2/r_1$  ratios indicate more sensitive systems, as

lower nanoparticle concentration is sufficient to darken MRI signal. Therefore, we anticipate that our EPS-coated MNP could increase the efficacy of MRI contrast compared to Endorem/Feridex, which has also a bacterial exopolysaccharide coating and similar clustering degree, given the respective hydrodynamic diameter. In the  $T_2$ -weighted MRI phantom images obtained for aqueous suspensions of MNP-DMSA-EPS (Figure 2C), it is visible that signal intensity decreases (darkening) with the increase of nanoparticle concentration, similar to what happens with dispersions of commercial superparamagnetic contrast agents.<sup>32</sup> Even for the lower iron concentration ( $0.1 \text{ mM} = 5.6 \mu\text{g/ml}$ ) there is a noticeable signal difference between water and the nanoparticles dispersion.

### Cell-nanoparticle interactions

Given the promising performance of MNP-DMSA-EPS, revealed by their relaxivities values, we further tested their efficacy as MRI negative contrast agent to label *in vitro* cultured cells. We have used HCT116 and ReNcell VM human cell lines as model systems to study interactions between MNPs and cells, namely, the impact on cell viability, iron uptake, intracellular localization of internalized nanoparticles and effect on MRI cell phantoms.

We aimed to assess the impact of Fucopol (EPS) coating on nanoparticle cytotoxicity. Therefore, for comparison purposes, we have evaluated MNP-DMSA-EPS, MNP-DMSA and EPS cytotoxicity profiles in parallel, using the MTT assay (colorimetric test based on cellular metabolic activity) for this purpose.

In the concentrations range tested, the two cell lines present distinct viability profiles after incubation with MNPs or EPS alone (Figure 3, Figure S4). After 48h of incubation with cells, MNP-DMSA, MNP-DMSA-EPS and EPS have an effect on the viability of HCT116 cells (Figure 3A), with relative half maximal inhibitory concentrations ( $IC_{50}$ ) of approximately  $55 \mu\text{g Fe/ml}$  for MNP-DMSA,  $82 \mu\text{g Fe/ml}$  for MNP-DMSA-EPS and  $96 \mu\text{g Fe/ml}$  for free EPS dissolved in the culture medium. Interestingly, HCT116 cell viability in presence of MNP-DMSA-EPS is lower than in the presence of MNP-DMSA or EPS alone. Stronger stress reaction of colon epithelial cancer cells to stabilized MNP compared to bare MNP or free stabilizer molecules were reported previously and justified by increased contact area between cells and stabilizer molecules upon contact with coated MNPs.<sup>33</sup> The different reactions to the same particle types are probably related with distinct sensitivity of the cell types to the tested materials and with nanoparticles exposure times. As Laurent *et al.* have previously demonstrated<sup>34</sup>, cytotoxicity profile resulting from the same nanoparticles, iron concentrations and incubation times is strongly dependent on cell type. On the other hand, exposition time is also an important factor that influences the response of a certain cell line to the presence nanoparticles. In some cases, longer incubation times promote the recovery of viability<sup>17</sup>, but in others it enhances the particles cytotoxic effect.<sup>17,35</sup> In our

study, 4h exposition of ReNcell VM cells to nanoparticles or EPS followed by 24h of recovery did not cause a pronounced decrease in the cell viability profile (Figure 3B, Figure S3), which is similar to the results found by other authors for primary human fetal neural precursor cells<sup>19</sup> and adipose-tissue

derived stem cells.<sup>35</sup> In the iron concentration range and exposition time used in our work, ReNcell VM cells viability is maintained above 80% and no IC<sub>50</sub> value is reached for the three materials

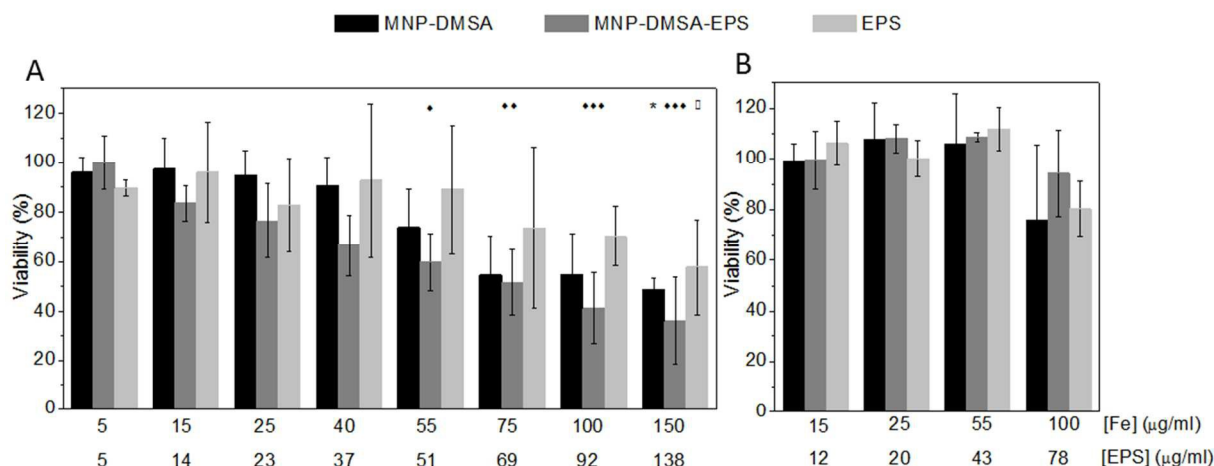


Figure 3. Cell cytotoxicity assay results for (A) HCT116 cell line after 48h exposition to nanoparticles and EPS and (B) ReNcell VM cell line after 4h exposition to nanoparticles and EPS plus 24h of recovery in fresh medium. Data is expressed as mean  $\pm$  standard deviation of at least two independent experiments. Different symbols indicate statistical difference of cells incubated with MNP-DMSA (\*), MNP-DMSA-EPS (♦) or EPS (□) compared to untreated control cells. Regular two-way ANOVA, followed by post-hoc pairwise comparison with Tukey's test was performed for statistical analysis using GraphPad Prism 6.0 software (USA); 1 symbol ( $p < 0.05$ ), 2 symbols ( $p < 0.005$ ), 3 symbols ( $p < 0.001$ ).

Microscopic observation of Prussian blue stained preparations (Figure 4A) allowed a preliminary evaluation of the particles labeling efficacy. No significant alteration of cell morphology was detected in MNP treated cells compared to untreated cells and no iron was detected inside the nucleus. MNP-DMSA-EPS are visible in both cell types as blue spots and aggregates distributed in the cytoplasm or attached to the cell surface. In ReNcell VM cells the blue spots are larger and more intense. This may be related with a stronger uptake of MNP-DMSA-EPS in ReNcell VM than in HCT116 cells or simply reflects the different incubation conditions used for the two cell types. Much less cellular uptake was observed when MNP-DMSA were used. Both particle types possess negative zeta potential

(that comes close to neutral after contact with culture medium), however MNP-DMSA-EPS present higher internalization in the two cell lines used in this work. Interactions between the cell membranes and nanoparticles' surfaces probably explain the first contact between MNPs and cell membrane, but given the size of the aggregates formed by MNP-DMSA-EPS, cell membrane-nanoparticle interactions may be facilitated. Moreover, the presence of fucose residues (which are known to be involved in cell-cell adhesion, cell-matrix adhesion, and cell-cell signaling processes<sup>36</sup>) may also contribute to enhanced uptake of MNP-DMSA-EPS compared to MNP-DMSA through interaction with cell surface receptors.

## ARTICLE

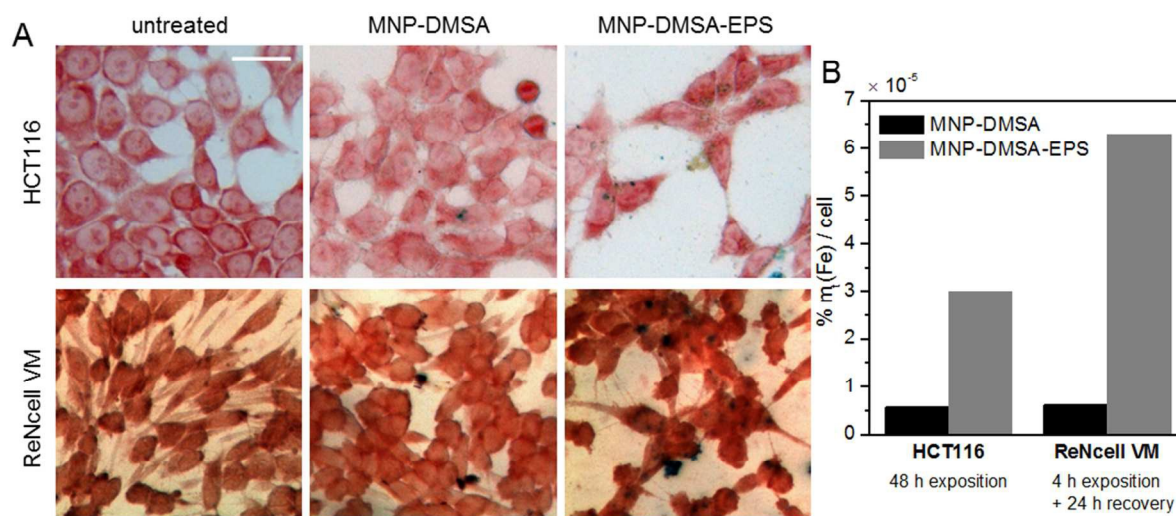


Figure 4. Observation and quantification of iron in cell cultures incubated with MNP-DMSA and MNP-DMSA-EPS. HCT116 cells were exposed to the nanoparticles for 48h. ReNcell VM cells were exposed to the nanoparticles for 4h, followed by a recovery period of 24h. (A) Bright field microscopy images of Prussian blue stained cells (scale bar: 10 $\mu$ m); (B) Proportion of total iron per cell, quantified by ICP.

Quantification of iron in cell fractions by ICP-AES after labeling (Figure 4B and Table 1) confirmed the Prussian blue observations. Since we have incubated HCT116 and ReNcell VM cells with different iron concentrations for each particle type, it was important to normalize the mass of cellular iron to the total mass of iron from MNPs in cell culture and to the number of cells. The normalized values show the same percentage of iron uptake by both cell lines when incubated with MNP-DMSA. However, after EPS conjugation to MNP-DMSA, a 5-fold and a 10-fold increase of cellular iron percent was observed for HCT116 and ReNcell VM cells, respectively (Figure 4B and Table 1). In this case, cellular iron is mainly due to internalized nanoparticles with a small contribution of nanoparticles adsorbed to the cell surface. On the other hand,

for MNP-DMSA, internalized and adsorbed nanoparticles contribute in equal proportions for the total iron found per cell (Figure S5 and Table S1). In ReNcell VM, although particle concentration and exposition time were lower, the double percentage of iron was found in the cellular fraction when compared with HCT116 cells (Table 1). According to the literature, fucose-galactose compounds mediate a pathway for the modulation of neuronal growth and morphology<sup>37</sup> and can be used in culture of neurons *in vitro* to induce neuronal growth and neurite elongation.<sup>38</sup> Fucose and galactose are the main components of Fucopol and thus this EPS may contribute to the enhanced MNP-DMSA-EPS uptake by neural stem/progenitor cells in relation to HCT116 cells.

Table 1. Uptake of iron by HCT116 and ReNcell VM after incubation with MNP-DMSA and MNP-DMSA-EPS.

Cell line	Incubation time with MNPs	MNP in the culture medium ( $\mu$ g Fe/ml)		Relative Fe uptake % mt(Fe)/cell ( $\times 10^{-5}$ )		Absolute Fe uptake (pg Fe/cell)	
		MNP-DMSA	MNP-DMSA-EPS	MNP-DMSA	MNP-DMSA-EPS	MNP-DMSA	MNP-DMSA-EPS
HCT116	48 h	54	46	0.57	3.00	1.22	8.35
ReNcell VM	4h + 24 h recovery	57	16	0.62	6.30	1.11	4.76

Comparison of our results with other studies is complex because several factors can influence labeling efficiency. These include, for example, cell type, concentration of iron,

incubation time, presence/absence of transfection agents, nanoparticle coating material or even the experimental protocol used for labeling efficiency evaluation. Previous reports dealing

with human colon cancer and neural stem cells treated with iron oxide nanoparticles coated with other polysaccharides observed iron internalization at different experimental conditions. Compared to our results, LS174T colon cancer cell line presented lower iron uptake upon incubation with dextran-coated MNP (0.006 pg Fe/cell, after incubation for 1h at 100  $\mu\text{g/ml}$ ) but enough to obtain MRI contrast *in vitro*.<sup>39</sup> More recently, oleic acid coated MNP encapsulated in the polysaccharide hyaluronan (HA) were shown to have an inhibitory effect towards several human cancer cell lines (including HCT116) and visible by MRI after injection in a murine intramuscular glioblastoma tumor model. While nanoparticles studied in our work were non-toxic at low iron concentrations, and do not inhibit growth, HA-MNPs originated negative viabilities at 10 – 500  $\mu\text{g Fe/ml}$  for 24, 48 and 72 h.<sup>40</sup> Regarding stem cells, the standard MRI labeling protocols are based in the utilization of a transfection agent (TA) together with commercially available iron oxide magnetic nanoparticles to promote internalization.<sup>6,18,41</sup> However, TAs are usually complex to use and cytotoxic.<sup>6,42</sup> Therefore, incubation of cells with the nanoparticles alone would be preferred. Some work has been done on modification of polysaccharide coatings, namely with positively charged chemical groups, to produce magnetic nanomaterials that provide enough labeling efficacy *per se*<sup>11,35</sup> but in this work we have evaluated the performance of MNP coated with the EPS Fucopol without any modification. We have seen that 4h of incubation with MNP-DMSA-EPS at 16  $\mu\text{g Fe/ml}$  allowed a labeling efficiency of 5 pg Fe/cell in ReNcell VM (Table 1), similar to what was reported previously for Feridex to label neural progenitor cells (75  $\mu\text{g Fe/ml}$ , 48 h, uptake of 5.1 pg Fe/cell)<sup>43</sup> and mesenchymal stem cells derived from the iliac crest bone marrow (25  $\mu\text{g Fe/ml}$ , 24h, uptake of 4.9 pg Fe/cell).<sup>44</sup> Adipose tissue-derived stem cells labeled with the experimental TMAD-03 (trimethylamine dextran-coated) MNPs (10  $\mu\text{g Fe/ml}$ , 1h) internalized slightly higher amounts of iron (~8 pg Fe/cell).<sup>35</sup> Our results thus show that, in particular for neural stem/progenitor cells, MNP-DMSA-EPS allow iron internalization efficiencies identical to those reported with commercial contrast agents, using lower iron concentrations, short incubation times and without using TA.

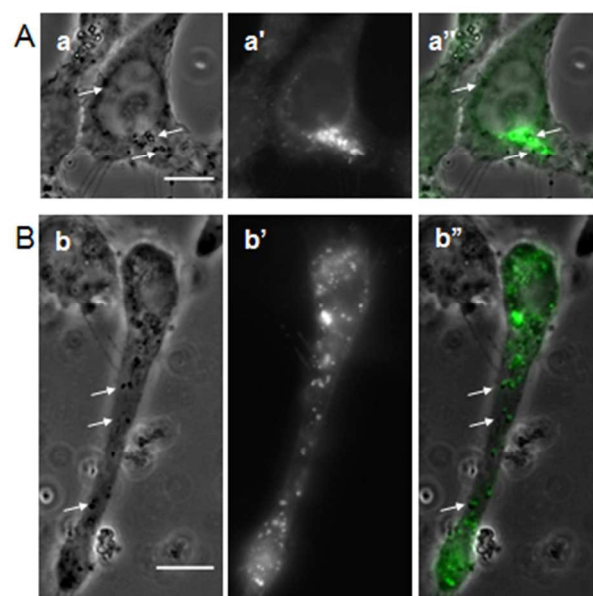


Figure 5. Localization of MNP-DMSA-EPS within (A) HCT116 cells and (B) ReNcell VM cells by microscopy. (a and b) bright field; (a' and b') GFP labeling of lysosomes and (a'' and b'') merged images. (Scale bar: 10  $\mu\text{m}$ ).

MNP-DMSA-EPS present hydrodynamic diameter in the range of 170 nm, therefore internalization by passive diffusion across the cell membrane would not be possible. The anticipated cell uptake mechanism is endocytosis, which is described for experimental and commercial MNPs in this size range.<sup>45,46</sup>

In order to confirm this assumption, a co-localization study of MNP-DMSA-EPS and lysosomes was performed, since these structures are the end-destination of materials internalized by endocytosis. Figure 5 shows bright field and fluorescence microscopy images of cells with GFP-labeled lysosomes after incubation with MNP-DMSA-EPS. It is clear that, in fact, nanoparticles (represented by black dots in bright field images) co-localize with lysosomes (visible as bright dots under fluorescence images) in the merged images (Figure 5A-a'' and Figure 5B-b''). Large MNP-DMSA-EPS aggregates that were not internalized are also visible in the bright field images as white-shining structures at the cell surface (Figure 5A-a) and in the extracellular space (Figure 5B-b).

#### Differentiation of MNP labeled neural stem/progenitor cells

Since ReNcell VM is a human neural stem/progenitor cell line, it is important to ensure that multipotency is maintained in the presence of the nanoparticles. After labeling with MNP-DMSA and MNP-DMSA-EPS, the cells were induced to differentiate for 14 days and the ability to generate neurons and glial cells was inspected by immunohistochemistry against neuronal ( $\beta$ -III Tubulin) and glial cell (GAFP) markers. As shown in Figure 6, no significant differences in expression of these markers in labeled cells (Figure 6 d-f and Figure 6 g-i) are observed when compared against unlabeled control cells (Figure 6 a-c), indicating that the presence of MNPs does not have an impact on multipotency. Our results are in accordance with previous

studies, where under similar culture conditions, but using MNPs with a different coating polymer, human neural precursor stem cells were shown to be able to retain the multilineage differentiation capability.<sup>19</sup>

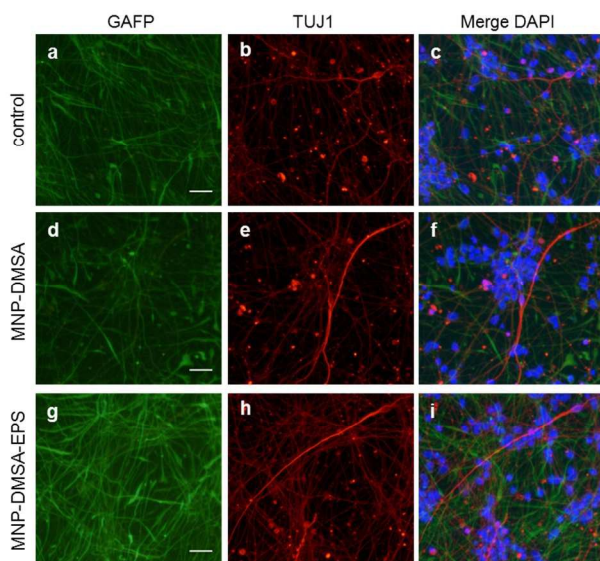
After the 14 days culture period, aggregates of MNP-DMSA-EPS are still visible in the culture (extracellular space and near the cell outer membranes), similar to what was observed in Prussian blue images (Figure 4A) suggesting long term retention of MNP, which is needed for *in vivo* cell tracking in cell-replacement therapies.

#### *In vitro* MRI of MNP-DMSA-EPS labeled cells

As concluded from the obtained relaxivities, MNP-DMSA-EPS are potentially efficient to produce contrast enhancement in MRI. In addition, ICP-AES analysis showed that these nanoparticles are internalized by both cell lines. Therefore, to evaluate MNP-DMSA-EPS efficacy to provide contrast enhancement after being internalized by the cells, agarose dispersions of labeled cells were studied by MRI. Hypointense regions are visible in T<sub>2</sub>-weighted MR images of MNP-DMSA-EPS labeled cells in contrast to unlabeled (control) cells (Figure 7), which confirms internalization (or surface adherence) of particles. However, in contrast to what is observed for HCT116 cells, labeling ReNcell VM cells with increasing particle concentrations originated increasingly darker images, as is evident in C<sub>1</sub>, C<sub>2</sub>, and C<sub>3</sub> phantoms and respective histograms in Figure 7A and Figure 7B. Figure 7C shows the quantification of the phantoms grey densities and confirms that for neural progenitor/stem cells, hypointensity increases with the concentration of nanoparticles used for labeling. Although for C<sub>1</sub> grey density is identical to that of unlabeled cells, for C<sub>2</sub> and C<sub>3</sub> signal losses of 20% and 43% were obtained, respectively. A linear relation was found for the variation of the integrated density of ReNcell VM MRI phantom images as a function of the iron concentration used for labeling ( $r^2 = 0.997$ ) (Figure S6).

Figure 6. Immunohistochemistry of post-labeled ReNcell VM cells at day 14 of culture. Scale bar: 20  $\mu$ m.

MRI labeling efficacy depends on the cell line and on the labeling conditions. Our results indicate that the conditions used in this work are adequate to label and detect ReNcell VM cells by *in vitro* MRI, but to label HCT116 cells further optimization may be required. In a previous work, we have shown MNP dose dependent contrast enhancement using the same colorectal cancer cell line and incubation period, with gum Arabic-coated MNP-DMSA at lower iron concentrations than in the present study<sup>20</sup>. Besides the distinct iron loads, differences in composition of the polysaccharide coatings could cause distinct interactions between cell membranes and particles, which justify the differences in detectability by MRI. The use of SPIONs to track and monitor stem cells after transplantation is important to help understanding the dynamics of cells proliferation, differentiation and migration. Therefore several approaches have been reported to develop effective MRI nanoprobes to label stem cells.<sup>6</sup> When compared to our results for neural stem cells, Yukawa *et al.*<sup>35</sup> obtained only subtle signal decrease in T<sub>2</sub>-weighted MRI phantom images of mesenchymal stem cells incubated with TMAD-03 at increasing iron concentrations (20, 30 and 50  $\mu$ g Fe/ml). On the other hand, Andreas *et al.*<sup>44</sup> reported MRI signal losses of approximately 20% and 50% for mesenchymal stem cells incubated for 24h with Resovist at 50 and 100  $\mu$ g Fe/ml, respectively. Interestingly, MNP-DMSA-EPS gave rise to similar signal losses at lower iron doses (Figure 7C). Eamegdool *et al.*<sup>19</sup> found out that the minimum iron uptake necessary for full identification of neural precursor stem cells neurospheres by *in vitro* MRI was between 5 and 10  $\mu$ g Fe/ml. We thus hypothesize the feasibility of neurosphere labeling with MNP-DMSA-EPS given the good labeling efficacy and MRI signal obtained in the referred range of iron concentrations, in our work.



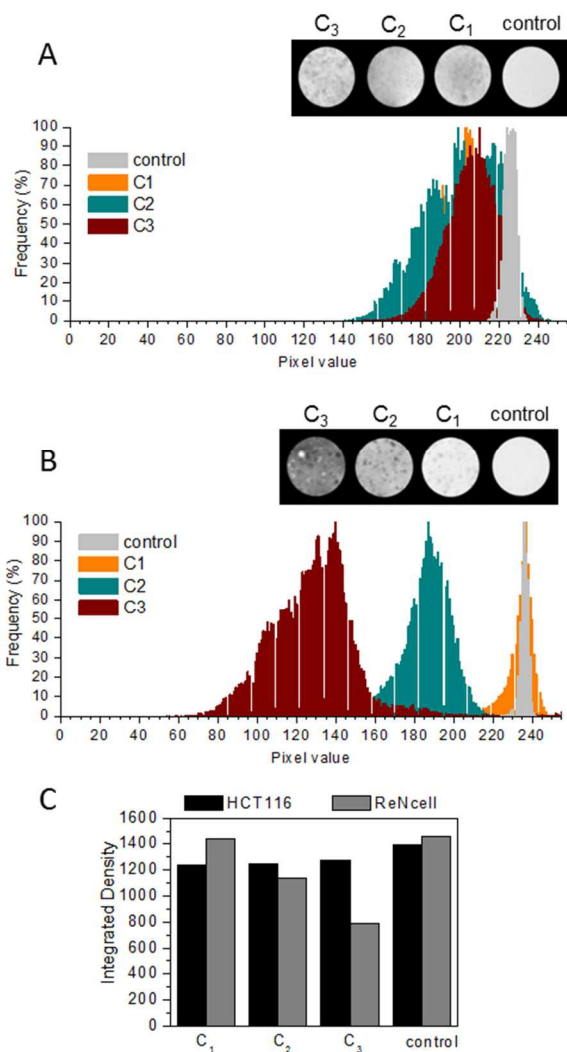


Figure 7. *In vitro* MRI images and corresponding histograms of (A) HCT116 and (B) ReNcell VM cells labeled with increasing concentrations of MNP-DMSA-EPS, from C<sub>1</sub> to C<sub>3</sub>, compared with unlabeled control cells. (C) Grey density quantification of images in (A) and (B). For HCT116 cells, C<sub>1</sub> = 61.5  $\mu\text{g Fe/ml}$ , C<sub>2</sub> = 82  $\mu\text{g Fe/ml}$ , C<sub>3</sub> = 102.5  $\mu\text{g Fe/ml}$ . For ReNcell VM cells, C<sub>1</sub> = 12  $\mu\text{g Fe/ml}$ , C<sub>2</sub> = 16  $\mu\text{g Fe/ml}$ , C<sub>3</sub> = 20  $\mu\text{g Fe/ml}$ .

## Conclusion

We have demonstrated the feasibility of a new biopolymer, the EPS Fucopol, as a coating material for iron oxide magnetic nanoparticles, and the suitability of the hybrid biopolymeric-magnetic particles for *in vitro* cell labeling by MRI. Fucopol is a biodegradable exopolysaccharide produced by *Enterobacter* A47 DSM 23139 when this bacterium is grown in a bioreactor using glycerol as a carbon source. The nanosystem preparation method was reproducible even when using different batches of EPS. Covalent coupling of the biopolymer onto DMSA-functionalized MNP was effective and produced aggregates with hydrodynamic size in the range of 170 nm and stable

negative zeta potential. The relaxivities ratio  $r_2/r_1$  is higher than the one reported for the commercial MRI contrast agent Feridex, with similar size and coated with the bacterial polysaccharide dextran. The *in vitro* cell culture assays showed that EPS-coated nanoparticles were internalized via endocytosis by the human cell lines HCT116 and ReNcell VM. Under the tested conditions, MNP-DMSA-EPS did not show cytotoxic effect in the neural stem/progenitor cell line nor affected their multipotency after 14 days of culture. In contrast to what was observed for HCT116, MNP-DMSA-EPS provided iron dose dependent MRI contrast enhancement in agarose dispersions of cells. The amount of cell-associated iron after ReNcell VM incubation with EPS-coated nanoparticles at the tested conditions is similar to the values reported for other stem cell lines labeled with Feridex for longer incubation periods and higher iron concentrations, suggesting potential applicability of our nanoparticles for stem cell labeling. Given the availability of carboxylic and hydroxyl groups in EPS, reporter and/or targeting molecules could be further conjugated to produce multimodal imaging agents with increased affinity for desired cell types. We conclude that EPS Fucopol-coated MNP are viable alternative tools to develop contrast agents for MRI techniques, being able to efficiently label cells through incubation without the need of additional transfection agents.

## Acknowledgements

The authors Dr. Carla Rodrigues for the ICP characterization, which was carried out at Laboratório de Análises, REQUIMTE, within Faculdade de Ciências e Tecnologia (Universidade Nova de Lisboa); Joana Silva for helping with preliminary MTT viability assays; and Pedro Silva for helping with colocalization study with GFP labeled lysosomes.

This work was partially funded by Fundação para a Ciência e Tecnologia/Ministério da Educação e Ciência (FCT/MEC), Portugal, through the projects PTDC/BBB-NAN/1812/2012, PTDC/EBB-BIO/102163/2008, PTDC/EBB-BIO/098961/2008, PTDC/EBB-BIO/118317/2010, PESt-C/EQB/LA0006/2011, PESt-OE/QUI/UI0100/2013, PESt-C/EQB/LA0006/2013, and the fellowships SFRH/BD/51112/2010 (S.I.C.J. Palma), SFRH/BPD/82056/2011 (C.A.V Rodrigues) and SFRH/BPD/72280/2010 (F. Freitas), The author A. Carvalho gratefully acknowledges the financial support from Strategic Project - LA 25-2013-2014 and the Portuguese Nuclear Magnetic Resonance Network (PTNMR).

## Notes and references

<sup>a</sup> UCIBIO, REQUIMTE, Departamento de Química, Faculdade de Ciências e Tecnologia, Universidade Nova de Lisboa, 2829-516 Caparica, Portugal.

<sup>b</sup> Department of Bioengineering and iBB - Institute for Bioengineering and Biosciences, Instituto Superior Técnico, Universidade de Lisboa, Avenida Rovisco Pais, 1049-001, Lisbon, Portugal.

## Journal Name

- <sup>c</sup> CENIMAT - IN, Departamento de Ciência dos Materiais, Faculdade de Ciências e Tecnologia, Universidade Nova de Lisboa, 2829-516 Caparica, Portugal.
- <sup>d</sup> Departamento de Biomateriales y Materiales Bioinspirados, Instituto de Ciencia de Materiales de Madrid, ICM/CSIC, 28049 Madrid, Spain
- <sup>e</sup> UCIBIO, Departamento Ciências da Vida, Faculdade de Ciências e Tecnologia, Universidade Nova de Lisboa, 2829-516 Caparica, Portugal.
- <sup>f</sup> CQE, Centro de Química Estrutural, Instituto Superior Técnico, Universidade de Lisboa, 1490-001 Lisboa, Portugal.
- Electronic Supplementary Information (ESI) available: Figures S1 – S3. See DOI: 10.1039/b000000x/
- 1 Y. Cohen and S. Y. Shoushan, *Curr. Opin. Biotechnol.*, 2013, **24**, 672–681.
  - 2 K. M. Krishnan, *IEEE Trans. Magn.*, 2010, **46**, 2523–2558.
  - 3 T.-H. Shin, Y. Choi, S. Kim and J. Cheon, *Chem. Soc. Rev.*, 2015.
  - 4 M. Modo, J. Kolosnjaj-Tabi, F. Nicholls, W. Ling, C. Wilhelm, O. Debarge, F. Gazeau and O. Clement, *Contrast Media Mol. Imaging*, 2013, **8**, 439–455.
  - 5 S. Uthaman, S. J. Lee, K. Cherukula, C.-S. Cho and I.-K. Park, *Biomed Res. Int.*, 2014, Article ID 959175.
  - 6 L. Li, W. Jiang, K. Luo, H. Song, F. Lan, Y. Wu and Z. Gu, *Theranostics*, 2013, **3**, 595–615.
  - 7 F. Freitas, V. D. Alves, C. a. V. Torres, M. Cruz, I. Sousa, M. J. Melo, A. M. Ramos and M. A. M. Reis, *Carbohydr. Polym.*, 2011, **83**, 159–165.
  - 8 C. Tassa, S. Y. Shaw and R. Weissleder, *Acc. Chem. Res.*, 2011, **44**, 842–52.
  - 9 B. Sivakumar, R. G. Aswathy, R. Sreejith, Y. Nagaoka, S. Iwai, M. Suzuki, T. Fukuda, T. Hasumura, Y. Yoshida, T. Maekawa and D. N. Sakthikumar, *J. Biomed. Nanotechnol.*, 2014, **10**, 885–99.
  - 10 F. Gao, Y. Cai, J. Zhou, X. Xie, W. Ouyang, Y. Zhang, X. Wang, X. Zhang, X. Wang, L. Zhao and J. Tang, *Nano Res.*, 2010, **3**, 23–31.
  - 11 J. Jo, I. Aoki and Y. Tabata, *J. Control. Release*, 2010, **142**, 465–73.
  - 12 S. A. Kalovidouris, C. I. Gama, L. W. Lee and L. C. Hsieh-Wilson, *J. Am. Chem. Soc.*, 2005, **127**, 1340–1.
  - 13 V. L. Dhadge, P. I. Morgado, F. Freitas, M. A. Reis, A. Azevedo, R. Aires-Barros and A. C. A. Roque, *J. R. Soc. Interface*, 2014, **11**, 20140743.
  - 14 S. Sun, H. Zeng, D. B. Robinson, S. Raoux, P. M. Rice, S. X. Wang and G. Li, 2004, **4**, 126–132.
  - 15 S. I. C. J. Palma, M. Marciello, A. Carvalho, S. Veintemillas-Verdaguer, M. D. P. Morales and A. C. A. Roque, *J. Colloid Interface Sci.*, 2015, **437**, 147–55.
  - 16 D. L. Morris, *Science*, 1948, **107**, 254–5.
  - 17 M. C. da Paz, M. de F. M. A. Santos, C. M. B. Santos, S. W. da Silva, L. B. de Souza, E. C. D. Lima, R. C. Silva, C. M. Lucci, P. C. Morais, R. B. Azevedo and Z. G. M. Lacava, *Int. J. Nanomedicine*, 2012, **7**, 5271–82.
  - 18 Jasmin, A. L. M. Torres, L. Jelicks, A. C. C. de Carvalho, D. C. Spray and R. Mendez-Otero, *Methods Mol. Biol.*, 2012, **906**, 239–52.
  - 19 S. S. Eamegdool, M. W. Weible, B. T. T. Pham, B. S. Hawckett, S. M. Grieve and T. Chan-ling, *Biomaterials*, 2014, **35**, 5549–64.
  - 20 S. I. C. J. Palma, A. Carvalho, J. Silva, P. Martins, M. Marciello, A. R. Fernandes, M. Puerto Morales and A. C. A. Roque, *Contrast Media Mol. Imaging*, 2015.
  - 21 R. M. Cornell and U. Schwertmann, *The Iron Oxides: Structure, Properties, Reactions, Occurrences and Uses*, Wiley-VCH GmbH & Co. KGaA, Weinheim, 2nd edn., 2003.
  - 22 A. Synytsya, *Carbohydr. Polym.*, 2003, **54**, 97–106.
  - 23 A. Barth, *Biochim. Biophys. Acta*, 2007, **1767**, 1073–101.
  - 24 M. M. Yallapu, N. Chauhan, S. F. Othman, V. Khalilzad-Sharghi, M. C. Ebeling, S. Khan, M. Jaggi and S. C. Chauhan, *Biomaterials*, 2015, **46**, 1–12.
  - 25 A. Salvati, A. S. Pitek, M. P. Monopoli, K. Prapainop, F. B. Bombelli, D. R. Hristov, P. M. Kelly, C. Åberg, E. Mahon and K. A. Dawson, *Nat. Nanotechnol.*, 2013, **8**, 137–43.
  - 26 M. Mahmoudi, I. Lynch, M. R. Ejtehadi, M. P. Monopoli, F. B. Bombelli and S. Laurent, *Chem. Rev.*, 2011, **111**, 5610–37.
  - 27 A. P. Roberts, Y. Cui and K. L. Verosub, *J. Geophys. Res.*, 1995, **100**, 17909.
  - 28 L. H. Bennett and E. Della Torre, *J. Appl. Phys.*, 2005, **97**, 10E502.
  - 29 H. Chen, J. Yeh, L. Wang, H. Khurshid, N. Peng, A. Y. Wang and H. Mao, *Nano Res.*, 2010, **3**, 852–862.
  - 30 J.-F. Berret, N. Schonbeck, F. Gazeau, D. El Kharrat, O. Sandre, A. Vacher and M. Airiau, *J. Am. Chem. Soc.*, 2006, **128**, 1755–61.
  - 31 B. Basly, D. Felder-Flesch, P. Perriat, C. Billotey, J. Taleb, G. Pourroy and S. Begin-Colin, *Chem. Commun.*, 2010, **46**, 985–987.
  - 32 J. Huang, L. Bu, J. Xie, K. Chen, Z. Cheng, X. Li and X. Chen, *ACS Nano*, 2010, **4**, 7151–60.
  - 33 C. A. Schütz, D. Staedler, K. Crosbie-Staunton, D. Movia, C. Chapuis Bernasconi, B. H. Kenzaoui, A. Prina-Mello and L. Juillerat-Jeanneret, *Int. J. Nanomedicine*, 2014, **9**, 3481–98.

- 34 S. Laurent, C. Burtea, C. Thirifays, U. O. Häfeli and M. Mahmoudi, *PLoS One*, 2012, **7**, e29997.
- 35 H. Yukawa, S. Nakagawa, Y. Yoshizumi, M. Watanabe, H. Saito, Y. Miyamoto, H. Noguchi, K. Oishi, K. Ono, M. Sawada, I. Kato, D. Onoshima, M. Obayashi, Y. Hayashi, N. Kaji, T. Ishikawa, S. Hayashi and Y. Baba, *PLoS One*, 2014, **9**, e110142.
- 36 P. S. Gene, *J. Cytol. Histol.*, 2012, **3**, 1000e102.
- 37 S. A. Kalovidouris, C. I. Gama, L. W. Lee and L. C. Hsieh-Wilson, *J. Am. Chem. Soc.*, 2005, **127**, 1340–1.
- 38 US 7858578 B2, 2005.
- 39 A. Moore, E. Marecos, A. Bogdanov and R. Weissleder, *Radiology*, 2000, **214**, 568–74.
- 40 D. Smejkalová, K. Nešporová, G. Huerta-Angeles, J. Srovátka, D. Jiráková, A. Gálisová and V. Velebný, *Biomacromolecules*, 2014, **15**, 4012–20.
- 41 J. A. Frank, B. R. Miller, A. S. Arbab, H. A. Zywicke, E. K. Jordan, B. K. Lewis, L. H. Bryant and J. W. M. Bulte, *Radiology*, 2003, **228**, 480–7.
- 42 N. Singh, G. J. S. Jenkins, R. Asadi and S. H. Doak, *Nano Rev.*, 2010, **1**, 1–15.
- 43 C.-C. V Chen, M.-C. Ku, J. D M, J.-S. Lai, D.-Y. Hueng and C. Chang, *PLoS One*, 2013, **8**, e56125.
- 44 K. Andreas, R. Georgieva, M. Ladwig, S. Mueller, M. Notter, M. Sittinger and J. Ringe, *Biomaterials*, 2012, **33**, 4515–25.
- 45 J. Pinkernelle, P. Calatayud, G. F. Goya, H. Fansa and G. Keilhoff, *BMC Neurosci.*, 2012, **13**, 32.
- 46 L. Matuszewski, T. Persigehl, A. Wall, W. Schwindt, B. Tombach, M. Fobker, C. Poremba, W. Ebert, W. Heindel and C. Bremer, *Radiology*, 2005, **235**, 155–61.